Editors' Suggestion Featured in Physics

Optical Tomography of Chemical Elements Synthesized in Type Ia Supernovae

I. R. Seitenzahl,[1,*] P. Ghavamian,[2] J. M. Laming,[3] and F. P. A. Vogt[4]
[1]*School of Science, University of New South Wales, Australian Defence Force Academy, Canberra, ACT 2600, Australia*
[2]*Department of Physics, Astronomy and Geosciences, Towson University, Towson, Maryland 21252, USA*
[3]*Space Science Division Code 7684, Naval Research Laboratory, Washington, D.C. 20375, USA*
[4]*European Southern Observatory, Av. Alonso de Córdova 3107, 763 0355 Vitacura, Santiago, Chile*

(Received 17 April 2019; published 22 July 2019)

We report the discovery of optical emission from the nonradiative shocked ejecta of three young type Ia supernova remnants (SNRs): SNR 0519-69.0, SNR 0509-67.5, and N103B. Deep integral field spectroscopic observations reveal broad and spatially resolved [Fe XIV] 5303 Å emission. The width of the broad line reveals, for the first time, the reverse shock speeds. For two of the remnants we can constrain the underlying supernova explosions with evolutionary models. SNR 0519-69.0 is well explained by a standard near-Chandrasekhar mass explosion, whereas for SNR 0509-67.5 our analysis suggests an energetic sub-Chandrasekhar mass explosion. With [S XII], [Fe IX], and [Fe XV] also detected, we can uniquely visualize different layers of the explosion. We refer to this new analysis technique as "supernova remnant tomography".

DOI: 10.1103/PhysRevLett.123.041101

Type Ia supernovae (SNe Ia) are the thermonuclear explosions of white dwarf (WD) stars. In spite of their importance as distance indicators in cosmology [1,2] and their major contribution to nucleosynthesis [3], no consensus has been reached on their explosion mechanism(s) and progenitor system(s) [4]. Even for the well-studied, nearby SN 2011fe, a comparison of the observations and synthetic spectral time series of the two leading explosion models has failed to produce a clear winner: the "single degenerate" delayed-detonation model of a $\sim 1.4\ M_\odot$ WD [5] and the "double degenerate" merger with a $\sim 1.1\ M_\odot$ [6] primary WD explain the observations nearly equally well [7].

An alternative approach to solving the SN Ia progenitor problem is via multiwavelength observations of supernova remnants (SNRs). Following the thermonuclear incineration of a white dwarf, the freshly synthesized heavy elements are ejected at high velocity. The supersonic expansion drives a forward shock into the surrounding interstellar medium and a reverse shock back into the remains of the supernova explosion, eventually heating the ejecta to x-ray emitting temperatures [8]. The most important parameters governing the evolution of SNRs are the chemical composition, kinetic energy, and mass of the ejecta, as well as the ambient medium density [9], all of which are closely linked to the explosion mechanism. As the supernova ejecta progressively ionize behind the reverse shock, zones of higher and higher atomic ionization are produced in succession behind this shock. Optical forbidden line emission from low-lying atomic transitions of these highly ionized atoms is expected. Many of these lines were first seen in the solar corona and are hence referred to as "coronal" lines.

The coronal [Fe XIV] magnetic dipole transition $3s^2 3p(^2P_{1/2} - {}^2P_{3/2})$ produces a green emission line at 5302.8 Å, with an emissivity that peaks in ionization equilibrium at temperatures near 2×10^6 K [10] and is produced over the range $7.0 < \log T < 7.5$ in the shock models presented below. Earlier detections of [Fe XIV] in SNRs were from "radiative" cloud shocks in ISM material ($\sim$300–500 km s^{-1}, where the postshock gas undergoes thermal instability and the shock dynamics are strongly affected by radiative cooling), such as those detected in Puppis A [11,12], N49 [13], and 1E0102.2-7219 [14], following model predictions [15]. In these cases, the sensitivity of the detectors has been the limiting factor in detecting optical [Fe XIV] from the much faster nonradiative shocks (>2000 km s^{-1}, no thermal instability) in both the swept up interstellar gas and reverse shocked ejecta.

As we show in this Letter, the superior sensitivity of the Multi Unit Spectroscopic Explorer (MUSE) Integral field spectrograph on the European Southern Observatory (ESO) Very Large Telescope (VLT) and the larger light gathering area of its 8.2 m mirror have now enabled the detection of faint optical coronal line emission in nonradiative shocks. Using public MUSE data from the ESO archive, we have discovered [Fe XIV] 5303 Å emission from the reverse shocks of the three youngest type Ia supernova remnants in the Large Magellanic Cloud (LMC) [16]: SNR 0519-69.0, SNR 0509-67.5, and N103B (SNR 0509-68.7). For further details on the observations, data reduction, and processing see the Supplemental Material [17].

To our knowledge this is the first detection of optical emission from the nonradiatively shocked ejecta of any

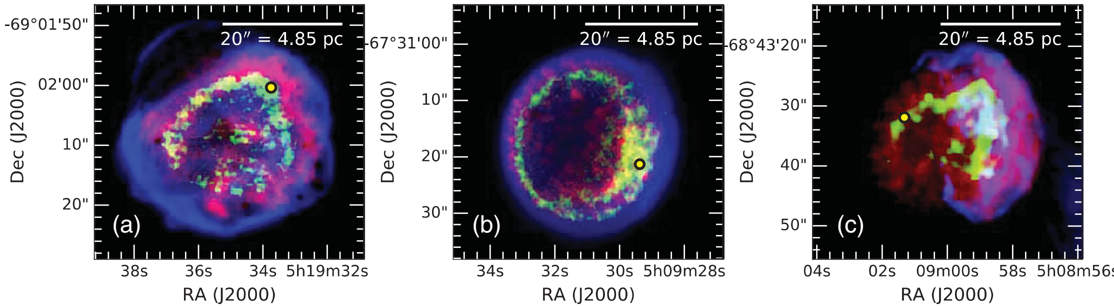

FIG. 1. RGB images of 0519-69.0 (a), 0509-67.5 (b), and N103B (c) showing in red x rays from Chandra ACIS, in blue *Hα* (MUSE), and in green [Fe XIV] (MUSE). The regions from which the spectra were extracted are indicated by the yellow dots.

type Ia supernova remnant. As expected, we find the peak of the [Fe XIV] emission, which appears as a narrow band in the interiors of the SNRs, immediately interior to the peak of the Fe *K* x-ray emission detected by the Chandra X-ray Observatory (see Fig. 1), since the reverse shock is propagating *inwards* in a Lagrangian sense. The detection of optical coronal line emission from pure nonradiative ejecta shocks of Type Ia SNRs opens a long sought window into the kinematic study of young Type Ia SNRs.

In the case of SNR 0519-69.0 (hereafter 0519) and SNR 0509-67.5 (hereafter 0509), the [Fe XIV] emission appears as a nearly circular shell [see Figs. 1(a) and 1(b)]. For N103B [Fig. 1(c)], the signal is contaminated by residuals from superimposed bright stars and the [Fe XIV] behind the reverse shock appears much more asymmetric. This is likely a consequence of the strong interaction of this SNR with high-density material on its western side [31]. The observed morphology of three nearly concentric shells of Balmer-line emission from the forward shock (blue) on the outside, with x-ray emission (red) from the hot, reverse shocked ejecta just inside the Balmer filaments, and coronal [Fe XIV] emission (green) inside of the x-ray emitting ejecta, is a beautiful confirmation of the extant theory of SNR evolution. To probe the kinematics of the iron-rich ejecta in each SNR, we have extracted [Fe XIV] line profiles (see Fig. 2) from selected regions (indicated in Fig. 1) of the three SNRs. Fitting single Gaussians and a linear continuum to the line profiles, we obtain velocity widths of $2460 \pm 100\ \mathrm{km\,s^{-1}}$ for 0519, $4370 \pm 100\ \mathrm{km\,s^{-1}}$ for 0509, and $3290 \pm 100\ \mathrm{km\,s^{-1}}$ for N103B.

The near spherical symmetry of 0519 and 0509 allows us to model them in one dimension (whereas the strongly asymmetric morphology of the [Fe XIV] in N103B does not), so in the remainder of this report we focus on these two SNRs for a quantitative analysis. While the approximate location of the reverse shock can be inferred from x-ray observations of the shocked ejecta [32], the resolved linewidth of the [Fe XIV] emission presented here allows us for the first time to directly determine the reverse shock speed—a new observational constraint. The radius of the peak of the [Fe XIV] emission, modeled as a spherical shell, is 2.86 ± 0.10 pc for 0509 and 2.36 ± 0.18 pc for 0519, respectively. To provide estimates of the total line fluxes we integrated the broad [Fe XIV] line over the full extent of the emission in each SNR and fit a single Gaussian to each line profile after subtracting a linear continuum. Corrected for extinction and reddening by dust, we obtain estimates of total line fluxes of $1.1 \times 10^{-14}\ \mathrm{erg\,cm^{-2}\,s^{-1}}$ for 0519 and $0.9 \times 10^{-14}\ \mathrm{erg\,cm^{-2}\,s^{-1}}$ for 0509.

A valuable constraint on the interpretation of our [Fe XIV] measurements is found in the time evolution of observed light echoes—the reflections of supernova light by interstellar dust sheets. Modeling of the light echoes [33]

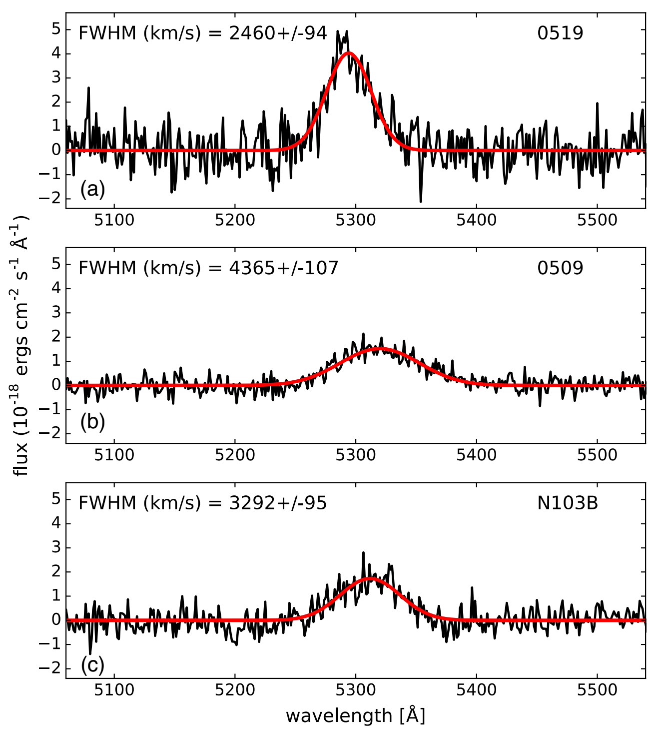

FIG. 2. [Fe XIV] 5303 line profiles for 0519-69.0 (a), 0509-67.5 (b), and N103B (c) extracted from the regions indicated (yellow dots with black edges) in Fig. 1. The apertures are circular with 0.8 arc sec radii, corresponding to 1.96 square arc sec areas (49 MUSE spaxels). Shown in red are best-fitting Gaussians to the data, determined by a least-squares minimization.

TABLE I. SNR models, parameters, and observations.

	0519: $E_{51}=1$; $M_{ej}=1.4$; $n_{ISM}=1.5$		0509: $E_{51}=1.5$; $M_{ej}=1.0$; $n_{ISM}=0.4$	
SNR	Observation	Model	Observation	Model
Age (yr)	600 ± 200 [33]	750	400 ± 120 [33] 310 ± 35 [35]	310
v_f (km s^{-1})	2770 ± 500 [32] 2650 [36]	2516	6500 ± 200 [35]	6539
R_f (pc)	4.0 ± 0.3 [32]	4.07	3.636 [35]	3.64
v_r (km s^{-1})		4057		5170
R_r (pc)		2.16		2.74
v_{exp} (km s^{-1})		1887		4766
$n_e t$ (10^{10} cm^{-3} s)	3.8 ± 0.3 [32]	3.7	0.85–3.4 [37] 1.4–1.6 [38]	0.315
T_e(K)	3.2e7 [32]	5.1e7	3.6 ± 0.6e7 [37] 4.6–5.8e7 [38]	1.97e7
R_{FeXIV} (pc)	2.18–2.55	2.8–2.9	2.76–2.96	2.81–2.85
W_{FeXIV} (km s^{-1})	2460 ± 94	3600	4365 ± 107	5117
F_{FeXIV} (erg cm^{-2} s^{-1})	1.1×10^{-14}		0.9×10^{-14}	
M_{FeXIV} (M_{sun})		0.03		0.015
M_{Fetot} (M_{sun})		0.38		0.515

Explosion energies E_{51} (10^{51} erg), ejecta masses M_{ej} (solar masses), ISM densities n_{ISM} (amu cm^{-3}), assumed age, modeled forward and reverse shock velocities and radii, and for 0519 ejecta ionization age and electron temperature, compared with observational values from literature references. Modeled and observed radii, width, [Fe XIV] 5303 flux, Fe mass associated with [Fe XIV] emission (includes [Fe X] also for 0509), and estimate of total SNR Fe mass.

allowed for an explosion model and SNR evolution independent determination of the SNR ages. These models placed 0519 at 600 ± 200 yr and 0509 at 400 ± 120 yr [33]. Further, since these two SNRs are located in the LMC, their distances are reliably known to be 50 kpc, with an uncertainty of only 2% [34]. This allows us to accurately relate angular size to physical size. The forward shock position and velocity can be inferred from the broad Balmer-line emission [35,36]. With reliable observational constraints on the age, forward shock position, and velocity, as well as reverse shock position and velocity, we are now in a position to limit explosion model parameters commensurate with the observational constraints.

Table I gives a summary of our SNR models based on [9] for 0519 and 0509, designed to match forward and reverse shock velocities (v_f and v_r) and radii (R_f and R_r) at the current epoch. The ejecta mass is M_{ej}, E_{51} is the explosion kinetic energy in 10^{51} erg, and n_{ISM} is the ambient density in amu cm^{-3}. For 0519 we take $M_{ej} = 1.4\ M_\odot$, $E_{51} = 1$, and a chemical composition 33% O, 12% Si, and 55% Fe mass, to match the results of x-ray analysis [32]. With $n_{ISM} = 1.5$ cm^{-3} taken to match the forward shock, we also get good agreement for the ejecta ionization age and electron temperature. Currently the reverse shock in 0519 has passed through approximately 95% of the ejecta (mass coordinate ~0.05), and the [Fe XIV]-emitting plasma is near mass coordinate 0.2, expanding with $v_{exp} = 1887$ km s^{-1}. For further details on our SNR hydrodynamical evolution model and ionization structure calculations see the Supplemental Material [17].

In the case of 0509, while adopting an explosion energy $E_{51} = 1.5$ and $n_{ISM} = 0.4$ cm^{-3} allows the forward shock radius and velocity to be matched as well as the emission measure of shocked ISM, a similar ejecta mass and composition to 0519 do not allow the Fe to ionize as far as Fe^{13+}. However, a smaller ejecta mass $M_{ej} = 1\ M_\odot$ allows the reverse shock to reach the ejecta core-envelope boundary, where the maximum ionization age occurs, earlier in the SNR evolution. This produces sufficient Fe^{13+} and Fe^{14+} here to generate brighter [Fe XIV] 5303 Å than [Fe XI] 7892 Å or [Fe X] 6376 Å, neither of which are unambiguously detected. We note that this high explosion energy is realistic and can be readily obtained from detonation of a 1 $M_\odot$ white dwarf with a 0.85 $M_\odot$ core consisting of 60% carbon and 40% oxygen (by mass) surrounded by a 0.15 $M_\odot$ shell of helium. Burning 0.5 $M_\odot$ of the core to iron-group elements (using the binding energy of ^{56}Ni) and the remainder of the star to intermediate mass elements (using the binding energy of ^{28}Si) gives a kinetic energy of 1.5×10^{51} erg, after accounting for the gravitational binding energy $E_g = -4.6 \times 10^{50}$ erg and the internal energy $E_{int} = 2.9 \times 10^{50}$ erg.

For the 1 $M_\odot$ ejecta model, the reverse shock in 0509 has passed through approximately 74% of the ejecta (mass coordinate 0.26) at the present time, and the [Fe XIV] emission originates from mass coordinates ~0.5–0.7, expanding with $v_{exp} = 4766$ km s^{-1}. Table I gives a summary of parameters connected with the [Fe XIV] emission for both remnants. There is good agreement between predicted and observed radii, with the observations giving a wider range of values. Presumably this arises partly from simple projection effects and partly from deviations of the SNR geometry from spherical symmetry. The linewidths, however, are overpredicted by about

10%–20%. The theoretical prediction is directly connected to the speed of the reverse shock and is possibly affected by the parametrization of the ejecta density profile by a uniform density core, or by clumping of the ejecta, which would slow down the reverse shock.

In Table I, the de-reddened fluxes in [Fe XIV] are given for the two remnants, with an estimate of the Fe mass in all charge states associated with the [Fe XIV] emission, coming from our ionization balance calculations. The final row of Table I gives an estimate of the total Fe in each remnant. To the Fe associated with [Fe XIV], we add the mass of currently unshocked ejecta ($0.18 \times 1.4 = 0.25\ M_\odot$ for 0519, $0.5 \times 1.0 = 0.5\ M_\odot$ for 0509), assumed all Fe, and for 0519 we add estimates of the shocked Fe mass seen in x rays [32]. For further details on the Fe mass estimate from the observed line flux see the Supplemental Material [17].

The characteristic velocity, distance, and time in our models depend on $(E_{51}/M_{\rm ej})^{1/2}$, $(M_{\rm ej}/n_{\rm ISM})^{1/3}$, and $M_{\rm ej}^{5/6}$ $E_{51}^{-1/2}$ $n_{\rm ISM}^{-1/3}$, respectively, so in Table I only $n_e t$ and T_e change if E_{51}, $M_{\rm ej}$, and $n_{\rm ISM}$ vary by the same factor. A factor of ∼4 increase in $n_e t$ is required to improve the agreement between predicted and measured $n_e t$ for 0509, which conflicts with established type Ia SN theory. If we solely increase $M_{\rm ej}$ and the age for 0509, $n_e t$ and T_e increase somewhat, but simultaneously v_f decreases and R_f increases, worsening the prediction of the forward shock trajectory. A modest increase in $M_{\rm ej}$ by ∼0.2–0.4 $M_\odot$ is allowable but would require the Fe to be embedded in He-rich ejecta to achieve the necessary degree of ionization. Such a near Chandrasekhar-mass scenario with unburned helium in the ejecta seems unlikely, but we cannot firmly rule out a near Chandrasekhar-mass explosion as, for example, in Ref. [37]. The larger mass makes the reverse shock slower, brings the Fe XIV width into better agreement with observations, and increases our estimate for the total Fe mass because the slower reverse shock has not propagated as far through the ejecta. However, the most satisfactory explanation for the $n_e t$ values is that the strong Si, S, Ar, and Ca emission seen in x rays [38] arises from ejecta clumps, with densities locally enhanced by a factor of ∼4. This gives a predicted $n_e t$ of order 10^{10} cm^{-3} s. Using an electron density of 4 cm^{-3} to interpret the emission measures given in [38] then yields masses of clumped ejecta of 0.068, 0.035, 0.007, and 0.003 $M_\odot$ for Si, S, Ar, and Ca, respectively, implying that a total of about 0.11 $M_\odot$ out of a total shocked ejecta mass of about 0.74 $M_\odot$ is clumped by a factor of about 4. Approximately 0.2 $M_\odot$ of the shocked ejecta mass is then visible in [Fe XIV] and [Fe XV]. Therefore, we favor the low mass-high explosion energy scenario.

A remaining question is why 0509 exhibits clumpy ejecta while 0519 apparently does not. Aside from being more than twice as old as 0509, 0519 is in a significantly more advanced evolutionary state due to its higher ambient density. Presumably, all ejecta clumps in 0519 have been destroyed by instabilities following reverse shock passage [39,40], whereas this has not yet occurred in 0509. Kelvin-Helmholtz and Richtmyer-Meshkov instabilities typically destroy clumps on a timescale of a few clump shock crossing times. Clumping of Fe in 0509 would remove the need for a He-dominated composition in the 1.4 $M_\odot$ model for explaining the Fe ionization, but poses problems in that clumping of SN ejecta is usually assumed to occur as a result of the inflation of Fe-Co-Ni bubbles by radioactivity. Fe should therefore be under-dense, though Ref. [41] interprets Fe knots as being due to ^{54}Fe.

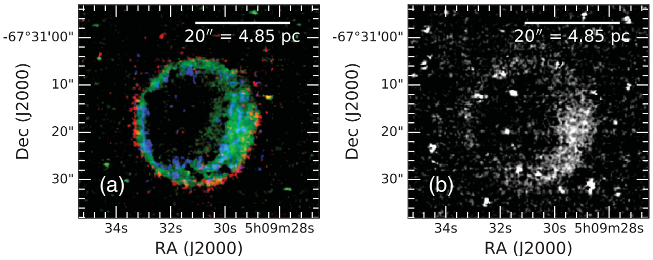

FIG. 3. (a) Left panel is RGB image of 0509-67.5 showing in red [S XII], in blue [Fe IX], and in green [Fe XIV]. (b) Right panel is image of 0509-67.5 in [Fe XV].

In addition to the ubiquitous [Fe XIV] emission, we also find two additional broad lines in 0509, which we identify as coronal [S XII] 7613.1, [Fe IX] 8236.8 [Fig. 3(a)], and [Fe XV] 7062.1 Å [Fig. 3(b)]. We also detect [Fe XV] 7062.1 Å in N103B. The presence of these further coronal lines in addition to [Fe XIV] opens the door to a new field of study: supernova remnant tomography, the study of spatially resolved, optical coronal line emission from nonradiative reverse shocks in type Ia supernova ejecta. The energetics of SNRs means that most of the emission from shocked ejecta is radiated at x-ray frequencies, observed with relatively poor spectral and spatial resolution due to technical limitations on the available instrumentation. Study of the optical coronal line profiles allows for the measurement of Doppler shifts and broadening. Furthermore, since the emission arises from much closer to the reverse shock than the x-ray emission, it is more sensitive to shock and preshock parameters. In contrast, the x-ray observations probe only the clumped ejecta, providing a less accurate picture of the spatial distribution of explosion products than the optical [Fe XIV] emission.

In the cases discussed here, the best match to the forward *and* reverse shocks pushes the SNR age to one end or the other of the uncertainty range coming from the light echoes and constrains the ejecta masses to around 1.4 $M_\odot$ for 0519 and likely to significantly below the Chandrasekhar mass for 0509 (∼1.0 $M_\odot$). In the absence of such information, the SNR age is much less constrained, with corresponding greater uncertainties in ejecta mass and explosion energy. Our dynamical models give a good match to the spectral properties of 0519 and 0509, with some clumping of the ejecta required for the latter SNR.

Last, we note that the observed light echo spectra enabled [42] to assign the supernova that gave rise to 0509 to the spectroscopic subclass of 1991T-like SNe Ia. Taking our explosion mass constraint at face value, this indicates that 1991T-like SNe Ia originate from detonations of sub-Chandrasekhar mass white dwarfs.

This research has made use of the following PYTHON packages: MATPLOTLIB [43], ASTROPY [44,45], a community-developed core PYTHON package for Astronomy APLPY [46], an open-source plotting package for PYTHON, ASTROQUERY [47], a package which provides a set of tools for querying astronomical web forms and databases, STATSMODEL [48] and BRUTIFUS [49], a PYTHON module to process data cubes from integral field spectrographs. This research has also made use of the ALADIN [50] interactive sky atlas, of SAOIMAGE DS9 [51] developed by Smithsonian Astrophysical Observatory, of NASA's Astrophysics Data System, and of NASA/IPAC Extragalactic Database (NED), which is operated by the Jet Propulsion Laboratory, California Institute of Technology, under contract with the National Aeronautics and Space Administration. I. R. S. was supported by the Australian Research Council through Grant No. FT160100028. P. G. acknowledges support from the rector funded visiting fellowship scheme at the University of New South Wales in Canberra. J. M. L. was supported by the NASA ADAP Program Grant No. NNH16AC24I and by Basic Research Funds of the Chief of Naval Research. F. P. A. V. acknowledges an ESO fellowship.

Author contributions—Conceptualization: I. R. S., P. G.; Formal analysis: I. R. S., J. M. L.; Investigation: I. R. S., P. G., J. M. L.; Methodology: I. R. S., P. G., J. M. L.; Project administration: IRS; Resources: F. P. A. V.; Software: I. R. S., J. M. L., F. P. A. V.; Visualization: I. R. S., J. M. L., F. P. A. V.; Writing–original draft: I. R. S., P. G., J. M. L., F. P. A. V.; Writing–review and editing: I. R. S., P. G., J. M. L., F. P. A. V.

*Corresponding author.
i.seitenzahl@adfa.edu.au

[1] A. G. Riess *et al.*, Astron. J. **116**, 1009 (1998).
[2] S. Perlmutter *et al.*, Astrophys. J. **517**, 565 (1999).
[3] I. R. Seitenzahl and D. M. Townsley, Nucleosynthesis in thermonuclear supernovae, in *Handbook of Supernovae*, edited by A. Alsabti and P. Murdin (Springer, Cham, New York, 2017), p. 1955, https://doi.org/10.1007/978-3-319-21846-5_87.
[4] W. Hillebrandt, M. Kromer, F. K. Röpke, and A. J. Ruiter, Front. Phys. **8**, 116 (2013).
[5] I. R. Seitenzahl, F. Ciaraldi-Schoolmann, F. K. Röpke, M. Fink, W. Hillebrandt, M. Kromer, R. Pakmor, A. J. Ruiter, S. A. Sim, and S. Taubenberger, Mon. Not. R. Astron. Soc. **429**, 1156 (2013).
[6] R. Pakmor, M. Kromer, S. Taubenberger, S. A. Sim, F. K. Röpke, and W. Hillebrandt, Astrophys. J. **747**, L10 (2012).
[7] F. K. Röpke *et al.*, Astrophys. J. **750**, L19 (2012).
[8] S. Reynolds and P. Supernova, Annu. Rev. Astron. Astrophys. **46**, 89 (2008).
[9] J. K. Truelove and C. F. McKee, Astrophys. J. Suppl. Ser. **120**, 299 (1999).
[10] P. Bryans, N. R. Badnell, T. W. Gorczyca, J. M. Laming, W. Mitthumsiri, and D. W. Savin, Astrophys. J. Suppl. Ser. **167**, 343 (2006).
[11] R. L. Lucke, J. C. Zarnecki, B. E. Woodgate, J. L. Culhane, and D. G. Socker, Astrophys. J. **228**, 763 (1979).
[12] R. G. Teske and R. Petre, Astrophys. J. **318**, 370 (1987).
[13] M. A. Dopita, I. R. Seitenzahl, R. S. Sutherland, F. P. A. Vogt, P. F. Winkler, and W. P. Blair, Astrophys. J. **826**, 150 (2016).
[14] F. P. A. Vogt, I. R. Seitenzahl, M. A. Dopita, and P. Ghavamian, Astron. Astrophys. **602**, L4 (2017).
[15] M. G. Allen, B. A. Groves, M. A. Dopita, R. S. Sutherland, and L. J. Kewley, Astrophys. J. Suppl. Ser. **178**, 20 (2008).
[16] J. P. Hughes, I. Hayashi, D. Helfand, U. Hwang, M. Itoh, R. Kirshner, K. Koyama, T. Markert, H. Tsunemi, and J. Woo, Astrophys. J. **444**, L81 (1995).
[17] See Supplemental Material at http://link.aps.org/supplemental/10.1103/PhysRevLett.123.041101, which includes Refs. [18–30], for details on the observations, data reduction, and processing.
[18] P. M. Weilbacher *et al.*, Astron. Astrophys. **582**, A114 (2015).
[19] W. Freudling, M. Romaniello, D. M. Bramich, P. Ballester, V. Forchi, C. E. Garciá-Dabló, S. Moehler, and M. J. Neeser, Astron. Astrophys. **559**, A96 (2013).
[20] E. L. Fitzpatrick, Publ. Astron. Soc. Pac. **111**, 63 (1999).
[21] E. F. Schlafly and D. P. Finkbeiner, Astrophys. J. **737**, 103 (2011).
[22] D. J. Schlegel, D. P. Finkbeiner, and M. Davis, Astrophys. J. **500**, 525 (1998).
[23] W. S. Cleveland, J. Am. Stat. Assoc. **74**, 829 (1979).
[24] F. P. A. Vogt, I. R. Seitenzahl, M. A. Dopita, and A. J. Ruiter, Publ. Astron. Soc. Pac. **129**, 975 (2017).
[25] A. J. S. Hamilton and C. L. Sarazin, Astrophys. J. **287**, 282 (1984).
[26] J. M. Laming and U. Hwang, Astrophys. J. **597**, 347 (2003).
[27] U. Hwang and J. M. Laming, Astrophys. J. **746**, 130 (2012).
[28] P. Ghavamian, J. M. Laming, and C. E. Rakowski, Astrophys. J. **654**, L69 (2007).
[29] R. A. Chevalier, Astrophys. J. **258**, 790 (1982).
[30] J. M. Laming, J. C. Raymond, B. M. McLaughlin, and W. P. Blair, Astrophys. J. **472**, 267 (1996).
[31] B. J. Williams, K. J. Borkowski, S. P. Reynolds, P. Ghavamian, J. C. Raymond, K. S. Long, W. P. Blair, R. Sankrit, P. F. Winkler, and S. P. Hendrick, Astrophys. J. **790**, 139 (2014).
[32] D. Kosenko, E. A. Helder, and J. Vink, Astron. Astrophys. **519**, A11 (2010).
[33] A. Rest *et al.*, Nature (London) **438**, 1132 (2005).
[34] G. Pietrzyński *et al.*, Nature (London) **495**, 76 (2013).

[35] L. Hovey, J. P. Hughes, and K. Eriksen, Astrophys. J. **809**, 119 (2015).

[36] L. Hovey, J. P. Hughes, C. McCully, V. Pandya, and K. Eriksen Astrophys. J. **862**, 148 (2018).

[37] C. Badenes, J. P. Hughes, G. Cassam-Chenaï, and E. Bravo, Astrophys. J. **680**, 1149 (2008).

[38] J. S. Warren and J. P. Hughes, Astrophys. J. **608**, 261 (2004).

[39] J. M. Pittard and E. R. Parkin, Mon. Not. R. Astron. Soc. **457**, 4470 (2016).

[40] S. Orlando, F. Bocchino, M. Miceli, X. Zhou, F. Reale, and G. Peres Astron. Astrophys. **514**, A29 (2010).

[41] C.-Y. Wang and R. A. Chevalier, Astrophys. J. **549**, 1119 (2001).

[42] A. Rest *et al.*, Astrophys. J. **680**, 1137 (2008).

[43] J. D. Hunter, Comput. Sci. Eng. **9**, 90 (2007).

[44] T. P. Robitaille *et al.* (Astropy Collaboration), Astron. Astrophys. **558**, A33 (2013).

[45] A. M. Price-Whelan *et al.* (Astropy Collaboration), Astron. J. **156**, 18 (2018).

[46] T. Robitaille and E. Bressert, Astrophysics Source Code Library ascl:1208.017 (2012).

[47] A. Ginsburg *et al.*, Astrophysics Source Code Library ascl:1708.004 (2017).

[48] S. Seabold and J. Perktold, in *Proceedings of the 9th Python in Science Conference (SCIPY 2010)*, p. 57, http://conference.scipy.org/proceedings/scipy2010/pdfs/seabold.pdf.

[49] F. P. A. Vogt, Astrophysics Source Code Library ascl: 1903.004 (2019).

[50] F. Bonnarel, P. Fernique, O. Bienaymé, D. Egret, F. Genova, M. Louys, F. Ochsenbein, M. Wenger, and J. G. Bartlett, Astron. Astrophys. Suppl. Ser. **143**, 33 (2000).

[51] W. A. Joye and E. Mandel, Astron. Soc. Pac. Conf. Ser. **295**, 489 (2003).